 doi:10.20944/preprints202210.0320.v1

Article

A Time-series Metabolomic Analysis of SARS-CoV-2 Infection in a Ferret Model

Avinash V. Karpe[1,2], Thao V. Nguyen[1,2], Rohan Shah[1,2], Gough G Au[3], Alexander J. McAuley[3], Glenn A. Marsh[3], Sarah Riddell[3], Seshadri S. Vasan[3,4], David J. Beale[1*]

[1] Land and Water, Commonwealth Scientific and Industrial Research Organisation, Ecosciences Precinct, Dutton Park, QLD 4102, Australia.
[2] Department of Chemistry and Biotechnology, School of Science, Computing and Engineering Technologies, Swinburne University of Technology, Hawthorn, VIC 3122, Australia.
[3] Commonwealth Scientific and Industrial Research Organisation, Australian Centre for Disease Preparedness, Geelong, VIC 3220, Australia
[4] University of York, Department of Health Sciences, York YO10 5DD, UK
* Correspondence: david.beale@csiro.au; Tel.: +61 7 3833 5774 (DJB).

Abstract: The global threat of COVID-19 has led to an increasing use of metabolomics to study SARS-CoV-2 infection in humans and animals. Despite this, understanding SARS-CoV-2's metabolome during an infection remains difficult and incomplete. Here, metabolic responses were characterized from sampled nasal washes collected from an asymptomatic ferret model (n = 20) at different time points before and after the SARS-CoV-2 challenge using an LC-MS-based metabolomics approach. Multivariate analysis of the nasal wash metabolome data resulted in several statistically significant features being observed. Despite no effects of gender or interaction between gender and time on the time course of SARS-CoV-2 infection, 16 metabolites were significantly different at every time point post-infection. Among these altered metabolites, the relative abundance of taurine was elevated post infection which could be an indication of hepatotoxicity, while the accumulation of sialic acids could indicate SARS-CoV-2 invasion. The pathway analysis identified several pathways influenced by SARS-CoV-2 infection. Of these, sugar, glycan, and amino acid metabolisms were the key altered pathways in the upper respiratory channel during infection. These findings provide some new insights into the progression of SARS-CoV-2 infection in ferrets at the metabolic level which could be useful for the development of early clinical diagnosis tools and new or repurposed drug therapies.

Keywords: COVID19; SARS-CoV-2; metabolomics; omics; animal models; ferret; host metabolic responses

1. Introduction

Highly transmissible and pathogenic coronavirus (CoV) infections are well-established sources of epidemics in humans and have caused global concerns. The severe acute respiratory syndrome CoV (SARS-CoV) first emerged in Guangdong, China in 2002 [1]. The SARS-CoV rapidly spread to 29 countries and caused 8096 infections and 774 deaths worldwide, according to the World Health Organization (WHO) [2]. The Middle East respiratory syndrome CoV (MERS-CoV) was first recorded in Saudi Arabia in 2012 and has rapidly spread to 27 countries [3]. As of May 2022, the total MERS-CoV infections reported globally is 2591 including 894 deaths, according to the WHO [4]. The novel coronavirus disease, COVID-19, caused by SARS-CoV-2 was first reported in Wuhan, China and has rapidly spread worldwide causing over 522 million cases [5]. Although the mortality rate is relatively low (1.2%), with, 5.94 million deaths reported between 1 January 2020 and 31 December 2021, analysis of excess mortality for this two-year period has led to an estimate of 17.1-19.6 million deaths at 95% uncertainty interval [6]. Current estimates are 6.5 million deaths recorded [5] and up to 26.5 million excess deaths globally [7].

Preprints (www.preprints.org) | NOT PEER-REVIEWED | Posted: 21 October 2022 doi:10.20944/preprints202210.0320.v1

The COVID-19 etiology is progressively being unraveled, but the underlying molecular mechanisms and the associated metabolic alterations remain poorly understood. The COVID-19 infection reflects a broad spectrum of patient symptoms. Several pathophysiological pathways are perturbed during the progression of disease. This complexity led us to investigate this exciting topic using metabolomics. Metabolomics studies the changes in holistic endogenous metabolites, presenting essential insights into a cell's metabolic state in response to physiological and pathological disturbances. Harnessing these metabolic outputs can potentially lead to the discovery of signature metabolic biomarkers relevant to pathogenesis. Such metabolic biomarkers could then be applied to personalized medicine, the development of public healthcare strategies, and/or the designing of Point-of-Care (PoC) testing regimens for more rapid testing [8, 9].

Most metabolomics studies related to COVID-19 have focused on the identification of new potential biomarkers of the disease. For example, Wu, *et al.* [10] reported altered energy metabolism (due to reduced malic acid of the TCA cycle) and hepatic dysfunction (due to reduced carbamoyl phosphate of the urea cycle and D-xylulose-5-phosphate of the pentose phosphate pathway). Barberis, *et al.* [11] suggested that monolaurin could have a potential defensive role against SARS-CoV-2 infection, and demonstrated that people with higher cholesterol levels are at a higher risk of developing SARS-CoV-2 infection. The dysregulation of macrophage, platelet degranulation, complement system pathways, and massive metabolic suppression have been reported in COVID-19 patient sera [12].

Dynamic shift of metabolic pathways is exhibited by living organisms to cope with various perturbations. Monitoring the dynamic metabolic changes during disease development has attracted increasing interest in recent years. Evidence from the literature suggests that the metabolomics studies based on time-series data could possibly provide insight into the interfacial stage between normal and diseased states and further facilitate the screening of biomarkers for early diagnosis. For example, Villoslada, *et al.* [13] studied the metabolomic signatures associated with disease severity in multiple sclerosis. Sphingomyelin and lysophosphatidylethanolamine were identified as putative biomarkers in the time series analysis for discriminating between multiple sclerosis patients and healthy individuals [13]. It was also reported that the levels of hydrocortisone, glutamic acid, tryptophan, eicosapentaenoic acid, 13S-hydroxyoctadecadienoic acid, lysophosphatidylcholines, and lysophosphatidylethanolamines were associated with more severe disease [13]. Jacyna, *et al.* [14] investigated the urine metabolic profiles of bladder cancer patients pre- and post-resection. It was reported that hippuric acid, pentanedioic acid and uridine could potentially be used for sample differentiation [14]. Huang, *et al.* [15] analysed the time-series lipidomics data to study the development of hepatocellular carcinoma in a hepatocarcinogenesis rat model. A ratio of lysophosphatidylcholine 18:1/free fatty acid (FFA) 20:5 was identified as the potential biomarker for hepatocellular carcinoma [15]. Li, *et al.* [16] used time-series metabolomics to study progressive stages of cholestatic liver fibrosis in mouse model. Taurocholic acid, tauromuricholic acid, lysophosphatidylethanolamine 20:2, sulfoglycolithocholic acid, and taurohyodeoxycholic acid were associated with the progression of the hepatocyte injury index, and docosahexaenoic acid, arachidonic acid, proline, leucine, and linoleic acid were associated with the progression of liver fibrosis index, liver hydroxyproline [16]. The metabolic profile during progression of cardiac heart failure was studied to discover potentially new biomarkers of the disease [17]. Twenty-three metabolites were altered in the rat model of myocardial infarction induced cardiac heart failure. The branched-chain amino acids, leucine and valine, were found to differentiate between the rat failing hearts and healthy hearts [17].

In our previous study, we analysed the nasal wash samples from SARS-CoV-2 infected ferrets [18]. Multivariate analysis of the acquired data identified 29 significant metabolites and three significant lipids in the nasal wash samples. The presence of viral shedding coincided with the challenge dose administered and significant changes in the citric acid cycle, purine metabolism, and pentose phosphate pathways, amongst others, in the nasal wash samples [18]. In the current study, the time-series metabolomics data from SARS-CoV-2 infected ferret model was analyzed to provide insights into the viral

Preprints (www.preprints.org) | NOT PEER-REVIEWED | Posted: 21 October 2022 doi:10.20944/preprints202210.0320.v1

progression and metabolic responses of ferrets to the virus infection. In addition, the study aimed to identify the gender-specific responses of male and female ferrets following SARS-CoV-2 exposure. For that purpose, ten male and ten female outbred ferrets (*Mustela putorius furo*) were challenged with SARS-CoV-2 via the intranasal route [19], and the nasal wash samples were collected for metabolomics analysis at six time points (3-days pre-infection and 3, 5, 7,9 and 14-days post-infection).

2. Materials and Methods

2.1. Ferret Challenge and Sample Collection

Ten male and ten female outbred ferrets (*Mustela putorius furo*, n = 20) at the age of 4 months were used for this challenge experiment. The study was reviewed by the Animal Ethics Committee (AEC) at the Australian Centre for Disease Preparedness (ACDP) (AEC 1990). All animal work in this study was conducted in the PC-4 containment facility at the ADCP in Geelong, Australia. Animal housing, husbandry, and handling for sample collections were as previously described [43]. Ferrets were acclimatized in cages at the facility for 7 days prior the experiment. During this period, animals were monitored daily and given food and water ad libitum, and environmental enrichment. Before the challenge, ferrets were implanted with a LifeChip Bio-Thermo transponder (Destron Fearing); subcutaneous temperature, rectal temperature and body weight were recorded.

SARS-CoV-2 (BetaCoV/Australia/VIC01/2020) was used for the challenge experiment which was provided by the Victorian Infectious Diseases Reference Laboratory (The Peter Doherty Institute, Melbourne, Australia) [44]. The viral preparation was conducted as the method described by Au *et* al [45]. All ferrets were challenged with SARS-CoV-2 VIC01 via the intranasal route (0.5 mL total volume diluted in PBS) at a target dose of approximately 9×10^4 $TCID_{50}$ (back-titered to 4.64×10^4 $TCID_{50}$). The inoculum was back-titrated by $TCID_{50}$ assay on Vero E6 cells to confirm the administered dose.

Following the virus challenge, ferrets were monitored daily for the presence of clinical signs (e.g., reduced-interaction score, fever, sneezing, coughing and respiratory disease). Animals were anesthetized for collection of nasal wash samples, as well as for the measurement of rectal temperature and body weight on days 3, 5, 7, 9 and 14 post virus challenge. All samples were rapidly frozen, and then gamma-irradiated (50 kGy) to inactivate the SARS-CoV-2 virus for safe removal of samples from the PC-4 containment laboratory. All samples were stored at −80 °C before extraction and metabolomics analysis. Reverse transcription qPCR was performed as per Marsh, *et al.* [46].

2.2. Metabolomics analysis

The metabolite extraction was carried out as previously described [18]. The frozen nasal wash samples were thawed in 100 µL PBS, and extracted with 450 µL of ice-cold methanol and ethanol solution (1:1, *v*/*v*) followed by 100 µL milliQ water. Samples were vortexed at 2000 rpm for 10 min before centrifugation at 20,000 g for 2 minutes at 4°C. The metabolite and lipid extracts were separated via the Captiva EMR-Lipid plate (2 mL, Agilent, Mulgrave, Australia). A rinse of 200 µL Water: Methanol: Ethanol (2:1:1) through the same Captiva EMR-Lipid tube was performed. The extracted solution was dried under nitrogen stream, followed by the resuspension in 50 µL 20% methanol (in water). The resuspended samples were re-vortexed at 1000 rpm at room temperature for 45 minutes and analyzed on an Agilent 6470 Liquid Chromatography Triple Quadrupole Mass Spectrometer (LC-QqQ-MS) (Agilent Technologies, Mulgrave, Vic, Australia) for central carbon metabolite (CCM) analysis. Furthermore, discovery metabolites (non-CCM) were analyzed using the same suspension on an Agilent 6546 Liquid Chromatography Time-of-Flight Mass Spectrometer (LC-QToF) with an Agilent Jet Stream source coupled to an Agilent Infinity II UHPLC system (Agilent Technologies, Santa Clara, CA, USA). The analysis was performed as per the previous method [47]. A series of blanks, mixed QC standards were prepared in the same way. Pooled biological quality control (PBQC) samples were prepared by combining 5 µL aliquots from each biological sample. Internal standards of 1

Preprints (www.preprints.org) | NOT PEER-REVIEWED | Posted: 21 October 2022 doi:10.20944/preprints202210.0320.v1

ppm L-phenylalanine (1-^{13}C) and succinic acid (1,4-$^{13}C_2$) were used. The residual relative standard deviation (RDS%) of the internal standards were 8.98% (L-Phenylalanine, 1-^{13}C) and 6.54% (Succinic Acid, 1,4-$^{13}C_2$).

2.3. Statistical analysis and data integreation

Identification of metabolites from acquired data was conducted using MassHunter Quantitative Analysis Software (v0B.10.0: Agilent Technologies, U.S.A). The acquired CCM data were first subtracted by blanks, then normalized to internal standards (L-phenylalanine ^{13}C and succinic acid ^{13}C). Untargeted metabolite data were normalized to reference ions (positive mode = ; negative mode =). The metabolomics data were subjected to further statistical analysis using multivariate statistics. The data were first imported, matched by sample identifiers (metadata), and log-transformed to normalize the data using SIMCA 16.02 (MKS Data Analytics Solutions, Uméa, Sweden). Partial Least Square-Discriminant Analysis (PLS-DA) was performed by finding successive orthogonal components from the SARS-CoV-2 isolate and sample type-specific datasets with maximum squared covariance and was subsequently used to identify the common relationships among the multiple datasets. All models were cross validated using CV-ANOVA in SIMCA, which is a diagnostic approach for assessing the reliability of PLS and OPLS models.

MetaboAnalyst 5.0 (Xia Lab, McGill University, Montreal, QC, Canada) was also used for the univariate and multivariate analysis, biomarker analysis, enrichment and metabolic pathway analysis [48]. Metabolite features with >50% missing values were excluded. A Log_{10} normalisation and auto scaling were applied to the filtered metabolite features. Metabolites with Benjamini–Hochberg adjusted *p*-value of ≤ 0.05 were considered to be statistically significant [49]. Chemical clusters based on structural similarity were created for metabolic examination using the ChemRICH analysis [50].

3. Results and Discussions

No clinical signs and perturbations on bodyweight were observed in ferrets after virus challenge. However, an increase of viral RNA shedding and changes of metabolites were recorded in nasal wash, indicating the infection of the virus in ferrets. The upper respiratory tract is one of the primary sites of SARS-CoV-2 infection [20, 21]. The current study involved nasal wash as the representative of the site of nasal tract to assess biochemical changes during SARS-CoV-2 infection in the ferret model.

3.1. Viral shedding following challenge

Viral RNA was detected in the nasal wash of 20 ferrets from 3 days post-infection (dpi) and continued to be detected at varying levels until 9 dpi **(Figure 1)**. The peak in viral RNA shedding was seen at 3 dpi and 7 dpi for all ferrets. A decline in viral RNA was seen at 5 dpi and 9 dpi for all ferrets. The viral RNA declined below the limit of quantification of the assay at 14 dpi at which point no viral RNA was detected in their nasal washes. Similar observation on viral RNA shedding have been reported in ferret model [19, 21, 22]. In humans, the mean time of viral shedding was reported to be 14 days [23, 24]. However, there is a wide variability of SARS-CoV-2 shedding among studies, reflecting the heterogeneity of human populations [25-27].

Preprints (www.preprints.org) | NOT PEER-REVIEWED | Posted: 21 October 2022 doi:10.20944/preprints202210.0320.v1

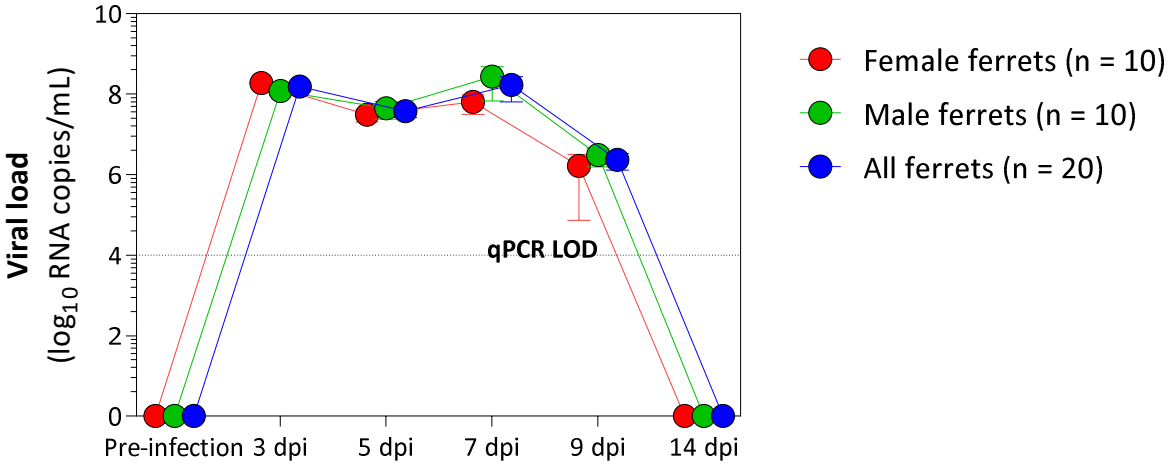

Figure 1. Viral RNA shedding in nasal washes collected from SARS-CoV-2 infected ferrets (n = 20). Red and green dots represent female (n = 10) and male ferrets (n = 10), respectively, while all ferrets (both males and females) are annotated in blue. SARS-CoV-2 RNA was detected in nasal wash samples from ferrets at 3, 5, 7, and 9 dpi. The dotted line represents the limit of detection (LOD) of the reverse transcription qPCR assay.

3.2. Central carbon metabolism variance in the nasal wash samples

The nasal washes from the infected ferrets were subjected to a central carbon metabolism metabolite screening via the LC-QqQ-MS method. The samples indicated the presence of 82 out of the 223 common polar metabolites from the central carbon metabolism and related pathways. The residual relative standard deviation (RSD%) of the internal standards was 8.99% (L-phenylalanine 1-^{13}C) and 6.54% (succinic acid 1,4-$^{13}C_2$). The RSD% of the QC standards **(Supplementary Table S1)** was <10% with the exception of lactic acid (RSD% = 11.07%). Within the PBQC samples, a total of 34 metabolites indicated an RSD% of <10% **(Supplementary Table S2)**.

This dataset was processed via an unsupervised statistical approach using Principal Component Analysis (PCA) **(Supplementary Figure S1)**. Any sub-data clustering was not evident from the PCA analysis. The grouped data were then analyzed using a supervised partial least squares discriminant analysis (PLS-DA) **(Supplementary Figure S2)** and orthogonal PLS-DA (OPLS-DA) **(Figure 2)** to explore metabolic differences in infected ferrets as a function of time. The PLS-DA analysis of nasal wash samples did not yield any better sub-data clustering. Whilst the PLS-DA dataset was found to be statistically non-significant (p-value > 0.05) when cross-validated **(Supplementary Table S3)**, the OPLS-DA model dataset was found to be statistically significant (p-value < 0.05, **Supplementary Table S4**).

Preprints (www.preprints.org) | NOT PEER-REVIEWED | Posted: 21 October 2022 doi:10.20944/preprints202210.0320.v1

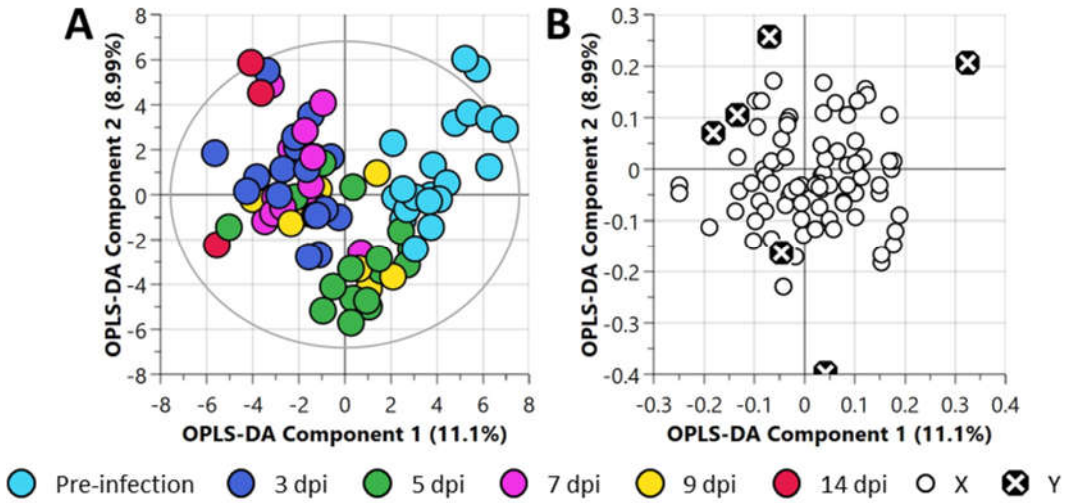

Figure 2. Orthogonal partial least square discriminant analysis (OPLS-DA) of the central carbon metabolism metabolite dataset of nasal wash samples collected from ferrets. **A.** OPLS-DA scatter plot, and **B.** OPLS-DA loadings plot. For this plot, R^2X (cum) = 0.453, R^2Y (cum) = 0.304, Q^2 = 0.108. The ellipse presented in panel **A** represents Hotelling's T2 confidence limit (95%). The colored circles in panel **A** represent each analyzed sample, while the black crossed circles in panel **B** indicate the average group position for each sample cluster, with the white circles representing the distribution of metabolite features between these groups.

3.3. Chemical and pathway analysis of the central carbon metabolism

The chemical analysis of the entire central carbon metabolism dataset indicated that monosaccharides, tricarboxylic acids (TCA), benzoic acids, organic dicarboxylic acids, fatty acids and conjugates, disaccharides, purines, amino acids and peptides, pyridines, carboxylic acids, pyrimidines, sulfonic acids, hydroxy acids, delta valerolactones, phosphate esters, keto acids, and benzamides were significantly (p-value < 0.05) enriched chemical classes.

The entire central carbon metabolism dataset was used to identify the most relevant pathways **(Supplementary Table S5)**. Several pathways including the pentose phosphate pathway, pentose and glucuronate interconversions, arginine biosynthesis, starch, and sucrose metabolism, D-glutamine and D-glutamate metabolism, alanine, aspartate and glutamate metabolism, citrate cycle, butanoate metabolism, valine, leucine, and isoleucine biosynthesis, amino sugar and nucleotide sugar metabolism, phenylalanine, tyrosine, and tryptophan biosynthesis, glyoxylate and dicarboxylate metabolism and nicotinate and nicotinamide metabolism were found to be significantly relevant **(**p-value < 0.05, **Figure 3)**. **Figure 4** illustrates the time-series observed for the central carbon metabolites contributing to these pathways.

Preprints (www.preprints.org) | NOT PEER-REVIEWED | Posted: 21 October 2022 doi:10.20944/preprints202210.0320.v1

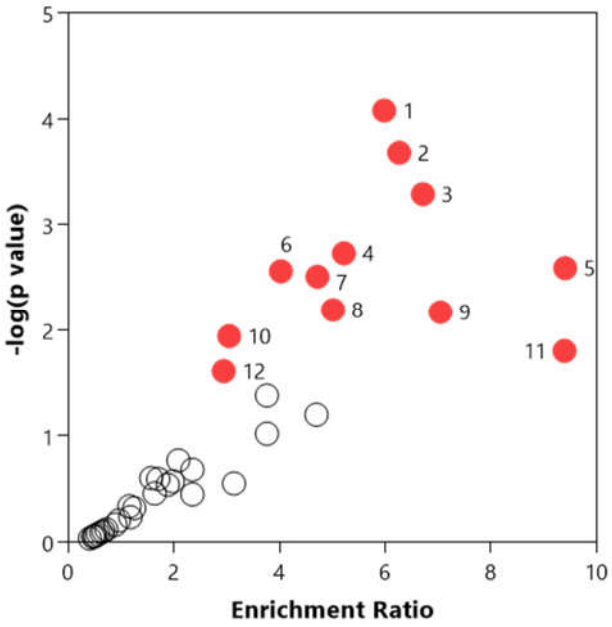

Figure 3. Relevant pathways identified using the central carbon metabolism dataset in nasal washes collected from ferrets. The red-colored circles represent significantly relevant pathways, while the white circles represent the non-significant pathways. *Noting*, 1: Pentose phosphate pathway, 2: Pentose and glucuronate interconversions, 3: Arginine biosynthesis, 4: Starch and sucrose metabolism, 5: D-Glutamine and D-glutamate metabolism, 6: Alanine, aspartate and glutamate metabolism, 7: Citrate cycle (TCA cycle), 8: Butanoate metabolism, 9: Valine, leucine and isoleucine biosynthesis, 10: Amino sugar and nucleotide sugar metabolism, 11: Phenylalanine, tyrosine and tryptophan biosynthesis, and 12: Glyoxylate and dicarboxylate metabolism.

In our previous study, pentose phosphate pathway, purine metabolism and citrate cycle were identified to be the key metabolite pathways in the ferret nasal cavity during SARS-CoV-2 infection [18]. The current study indicated that the sugar and glycan metabolism pathways leading from and to the non-oxidative parts of energy pathways were of key importance in the upper respiratory channel during the SARS-CoV-2 infection. Particularly, in our studies, pentose phosphate pathway (PPP) has shown to play a key role during SARS-CoV-2 infection. Recently reported proteomic study indicated that the enzymes such as transketolase (TKT) and transaldolase 1 (TALDO1) which contribute towards the non-oxidative part of PPP, were upregulated in the cells infected with SARS-CoV-2 [28]. Due to this phenomenon, biochemicals such as 2-deoxy glucose (2DG) and benfooxythiamine (BOT) which inhibit the non-oxidative pathways of PPP, have shown to inhibit SARS-CoV-2 replication [28, 29]. In addition to this, recent correlation network analysis in patients with COVID-19, has also shown that in addition to the viral infection, the upper respiratory microbiota also gets affected during SARS-CoV-2, which in turn has been shown to be correlated with the upregulation of pathways such as PPP [30]. Although we did not study the impact of SARS-CoV-2 infection on nasal microbial population and metabolism, a further study of host-microbiome-virus interactomics is expected to shed more light on this biochemical mechanism.

PPP associated pathways such as glycan metabolism (reflected through the pentose and glucuronate interconversions) and amino sugar and nucleotide sugar metabolism appeared to be key pathways in ferret nasal cavity during SARS-CoV-2 infection. Some of the early genomic studies have shown that the SARS-CoV-2 triggered surface protein receptors (STSPRs) such as Ephrin type-A receptor 6 (EPHA6) are differentially expressed in the human lungs. The EPHA6 proteins have been indicated to be enriched for pentose and glucuronate interconversions [31]. Our study experimentally confirms the outputs of the bioinformatics-based observations of Forst, *et al.* [31] that in the ferret upper

 doi:10.20944/preprints202210.0320.v1

respiratory tract, the pentose and glucuronate interconversions generally upregulate, particularly around 5-7 dpi **(Figure 4B)**. It has been shown in the poultry studies that the infection stress due to high density stocking elevated the pentose and glucuronate interconversion pathway, during the upregulated interleukin (IL)-1β and IL-10 activities in the tracheal barrier and plasma, possibly providing immune response against the infection [32]. Furthermore, the treatment regimen involving bleomycin + pirfenidone drug supplementation for treating the lung fibrosis condition in mice indicated an upregulated pentose and glucuronate interconversion pathway. This study indicated the positive role of this metabolic pathway in providing an immune response to host during respiratory disorders [33]. Thus, our study indicated a likely increased immune response to SARS-CoV-2 infection. However, a further proteomic study would be able to further highlight the importance of this pathway in conferring its role towards host immune response.

Similar to the pentose and glucuronate interconversion pathway, a recent bioinformatics study indicated that the amino sugar pathway expression has been associated with immunity-related pathways upon the expression of SARS-CoV-2 transmembrane serine protease 2 (TMPRSS2) during COVID-19 [34]. This is an important aspect as it has been shown that the blood plasma amino sugars are key parts of the bio-signaling N-acetyl glycoproteins such as GlycA and GlycB and are important in providing the immune response during SARS-CoV2 infection in the patients [35]. Furthermore, it has also been observed that glutaminolysis and glycolysis are essential for virus replication during SARS-CoV-2 infection, and inhibiting these pathways is important to counter virus replication [36]. Our observations of depleted glutamine and glutamate pathways **(Figure 4E)** indicated a possibly elevated immune response in the respiratory tract cells of the ferrets. Our metabolic output confirms the output of these genomics-based studies through metabolic output. Also, the time-series observations indicated an increased immune response by 7 dpi in ferret model. However, the proteomic studies will be able to provide further confirmation of these observations.

Preprints (www.preprints.org) | NOT PEER-REVIEWED | Posted: 21 October 2022 doi:10.20944/preprints202210.0320.v1

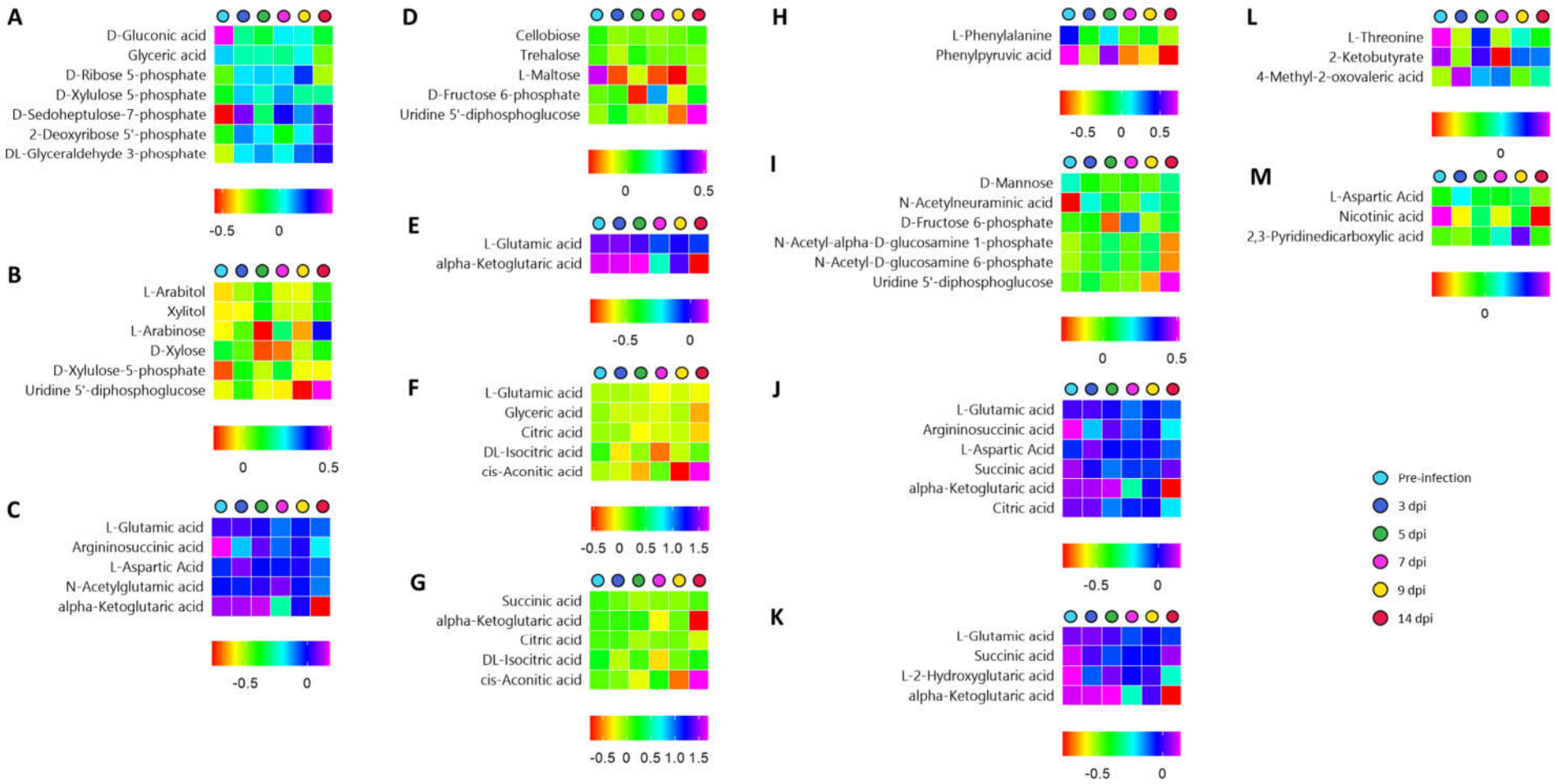

Figure 4. Time-series observed for metabolites related to the 13 significantly relevant central carbon metabolic pathways. **A.** Pentose phosphate pathway, **B.** Pentose and glucuronate interconversions, **C.** arginine biosynthesis, **D.** starch and sucrose metabolism, **E.** D-glutamine and D-glutamate metabolism, **F.** glyoxylate and dicarboxylate metabolism, **G.** citrate cycle, **H.** phenylalanine, tyrosine and tryptophan biosynthesis, **I.** amino sugar and nucleotide sugar metabolism, **J.** alanine, aspartate and glutamate metabolism, **K.** butanoate metabolism, **L.** valine, leucine and isoleucine biosynthesis, and **M.** nicotinate and nicotinamide metabolism.

 doi:10.20944/preprints202210.0320.v1

3.4. Multivariate analysis of the central carbon metabolism and discovery metabolites

The posthoc ANOVA indicated the presence of 28 significant central carbon metabolism metabolites (FDR-adjusted p-value ≤ 0.05) in nasal washes **(Supplementary Table S6)**. The samples were further analysed using a Liquid Chromatography Quadrupole Time-of-Flight Mass Spectrometry (LC-QToF-MS) method to identify the discovery metabolites. Eight significant metabolic features were identified **(Supplementary Table S7)**. The significant metabolites were used to identify the most relevantly disturbed metabolic pathways due to the viral infection. These significant metabolites were then used to identify the most significantly disturbed metabolic pathways. While the phenylalanine, tyrosine and tryptophan biosynthesis, phenylalanine metabolism, and butanoate metabolism were significantly ($p < 0.05$) enriched and impacted **(Supplementary Table S8)**, other pathways such amino sugar and nucleotide sugar metabolism and citrate cycle were significantly enriched and impacted, respectively.

3.5. Time-series metabolomics analysis of the progression of SARS-CoV-2 infection

A two-way analysis of variance (ANOVA) was then conducted to decompose the raw data to further determine the contribution of two independent parameters (gender and time) and their interaction. The abundance of several metabolic features was significantly affected by time **(Figure 5)**. No metabolic features were significantly affected by gender or interaction between gender and time.

The thirty significant features included D-sedoheptulose-7-phosphate, N-acetyl D-galactosamine, uric acid, vanillic acid, taurine, phenylpyruvic acid, nicotinic acid, L-2-hydroxyglutaric acid, 2,3-dihydroxyisovalerate, D-pantothenic acid, malonic acid, 2,3-dihydroxybenzoic acid, L-maltose, L-malic acid, N-acetylneuraminic acid, m-hydroxybenzoic acid, N-acetyl-alpha-D-glucosamine 1-phosphate, N-acetyl-D-glucosamine 6-phosphate, citramalic acid, myo-inositol, L-sorbose, L-phenylalanine, succinic acid, L-serine, 3-hydroxyanthranilic acid, mevalonic acid, 2-deoxycytidine 5-diphosphate, isopentyl acetate, D-galactosamine, and glyceric acid.

Of these metabolites, taurine, N-acetyl D-galactosamine, N-acetylneuraminic acid, D-sedoheptulose 7-phosphate and L-galactosamine increased from pre-infection to 14 dpi. Other metabolites such as L-maltose, 2,3-dihydroxyisovalerate, nicotinic acid, D-pantothenic acid, m-hydroxybenzoic acid, and 2-hydroxyglutaric acid decreased as the infection progresses. Vanillic acid, uric acid and 2,3-dihydroxybenzoic acid decreased at 3 dpi, showed a slight increase at 5 dpi, and then decreased again. Myo-inositol, L-sorbose, succinic acid and L-phenylalanine decreased post challenge.

Preprints (www.preprints.org) | NOT PEER-REVIEWED | Posted: 21 October 2022 doi:10.20944/preprints202210.0320.v1

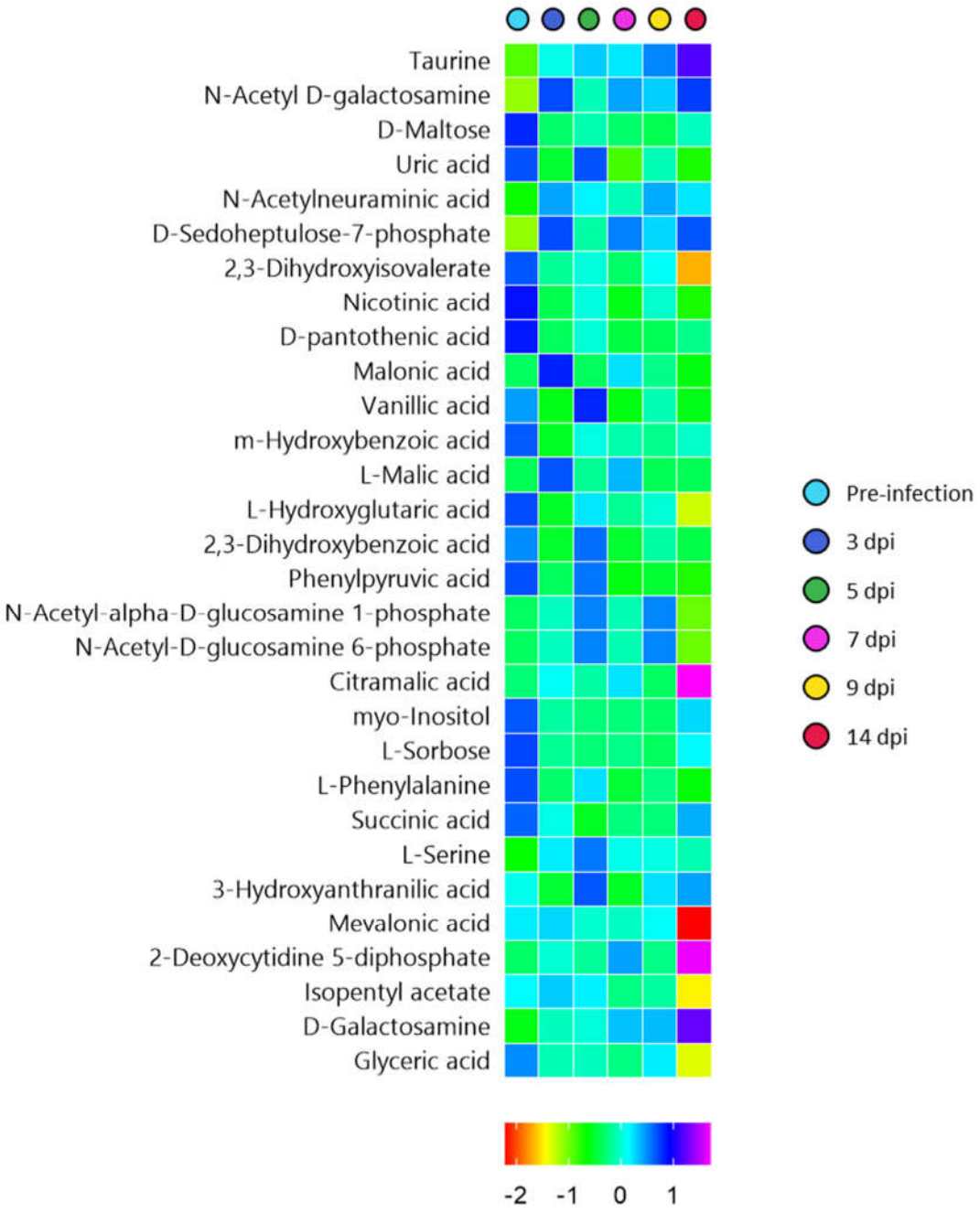

Figure 6. Heatmap representing the significant metabolites that were found to significantly vary identified using two-way analysis of variance.

The up- and down-regulation of these metabolites according to infection time could be signatures of viral infection on the host. For example, the elevated taurine could be an indication of hepatotoxicity due to SARS-CoV-2 infection. These observations are consistent with previous studies of SARS-CoV-2, indicating the role of elevated taurine in liver injury, which could be due to high prevalence of abnormal aminotransferase enzymes [37]. Several members of the CoV family use sialic acids, such as N-acetylneuraminic acid and N-acetyl-D-galactosamine, which are abundantly expressed on the host cell surface of the respiratory tract, as attachment points [38, 39]. Elevated sialic acids in the current study indicates SARS-CoV-2 invasion. Particularly high levels of sialic acids were found at 3 dpi and 7 dpi, when the viral load was at the peak. Nicotinic acid with reported anti-inflammatory properties is thought to influence the immune response [37]. Decline in nicotinic acid at 3 dpi and 7 dpi indicates infectious nature of SARS-CoV-2

 doi:10.20944/preprints202210.0320.v1

represented by high levels of viral load. Reduced levels of pantothenic acid could cause lack of vitamin B5 and thus, compromise the mitochondrial energy metabolism [40]. Bruzzone, *et al.* [41] reported increased levels of phenylalanine and succinic acid in COVID-19 patients. On the contrary, the levels of these metabolites were found to decrease in the current study. Nevertheless, this may all be related to dysregulation of hepatic central carbon metabolism. Li, *et al.* [42] investigated the use of uric acid as a prognostic marker of COVID-19 patients. Declined levels of uric acid from 7 dpi in nasal samples of ferrets in the current study align well with the observations by Li, *et al.* [42]. Hence, this metabolite could be used as a marker to assess the severity of COVID-19 for both human and animal models.

4. Conclusions

The present study demonstrated the use of ferret model to study the progression of SARS-CoV-2 infection and metabolic responses of the host to the infection. The viral RNA was detected at 3 dpi and remained detectable until 9 dpi with the absence of clinical signs, indicating that ferrets are an appropriate model for studies of asymptomatic SARS-CoV-2 infection. Along with the change in viral shedding, differences in metabolic responses of the host to different stages of the infection were observed via a time-series metabolomic analysis. This highlighted the power of metabolomics approaches for the systemic characterization of the disease via non-invasive sampling. In addition, this approach provided some metabolite candidates (e.g., uric acid, sialic acids) that could be used as a prognostic indicator SARS-CoV-2 infection and a biomarker to access the disease severity of COVID19.

Supplementary Materials: Figure S1: Principal component analysis (PCA) of the central carbon metabolism metabolite dataset of nasal wash samples collected from ferrets; Figure S2: Partial least square discriminant analysis (PLS-DA) of the central carbon metabolism metabolite dataset of nasal wash samples collected from ferrets; Table S1: Composition of QC mix standards (1 ppm) applied to assess the variability of the LC-QQQ-MS metabolomic analysis for central carbon metabolites; Table S2: Composition of PBQC metabolites applied to assess the variability of the LC-QQQ-MS metabolomic analysis for central carbon metabolites; Table S3: Cross-validation (CV)-ANOVA of the PLS-DA metabolomics model (Figure S2); Table S4: Cross-validation (CV)-ANOVA of the OPLS-DA metabolomics model (Figure 2); Table S5: Pathway enrichment analysis of the central carbon metabolic pathways using the central carbon metabolism dataset; Table S6: Multivariate ANOVA analysis of a metabolomics-derived dataset of nasal wash samples collected from ferrets at several time-points; Table S7. Significant discovery metabolites observed through LC-QTOF-MS analysis. Table S8: Pathway enrichment and impact analysis of a metabolomics-derived dataset of nasal wash samples collected from ferrets.

Author Contributions: Conceptualization, D.J.B. and S.S.V.; methodology, D.J.B.; investigation and analysis, A.K., T.V.N and R.S.; writing—original draft preparation, A.K., T.V.N., R.S., S.S.V., and D.J.B.; writing—review and editing, all authors; project administration, D.J.B.; funding acquisition, S.S.V. All authors have read and agreed to the published version of the manuscript.

Funding: This research was supported by funding (applicant: S.S.V.) from the Coalition for Epidemic Preparedness Innovations (CEPI), CSIRO's Future Science Platforms, and the US FDA's Medical Countermeasures initiative (contract number 75F40121C00144). The authors acknowledge the Australian Centre for Disease Preparedness, in providing their National Collaborative Research Infrastructure Strategy (NCRIS)-funded facility used in the completion of the animal studies. The article reflects the views of the authors and does not represent the views or policies of the funding agencies including the FDA.

Institutional Review Board Statement: This study was reviewed and approved by the Animal Ethics Committee (AEC) at the CSIRO Australian Centre for Disease Preparedness (AEC approval number #1989).

Informed Consent Statement: Not applicable.

Data Availability Statement: The metabolite data of this study are not publicly available due to animal ethics and intellectual property restrictions. The data are available on request from the corresponding author.

Acknowledgments: The authors thank their colleagues at the Australian Centre for Disease Preparedness for the animal studies from which samples were collected for metabolomics analysis.

Conflicts of Interest: The authors declare no conflict of interest.

Appendix A: Supplementary data.

References

1. WHO. Update 95 - SARS: Chronology of a serial killer. Available online: https://www.who.int/emergencies/disease-outbreak-news/item/2003_07_04-en (accessed on
2. WHO. Summary of probable SARS cases with onset of illness from 1 November 2002 to 31 July 2003. Available online: https://www.who.int/publications/m/item/summary-of-probable-sars-cases-with-onset-of-illness-from-1-november-2002-to-31-july-2003 (accessed on
3. WHO. Middle East respiratory syndrome coronavirus (MERS-CoV). Available online: https://www.who.int/news-room/fact-sheets/detail/middle-east-respiratory-syndrome-coronavirus-(mers-cov) (accessed on
4. WHO. Middle East respiratory syndrome coronavirus (MERS-CoV) - Qatar. Available online: https://www.who.int/emergencies/disease-outbreak-news/item/2022-DON370 (accessed on
5. WHO. Weekly epidemiological update on COVID-19 - 25 May 2022. Available online: https://www.who.int/publications/m/item/weekly-epidemiological-update-on-covid-19---25-may-2022 (accessed on
6. Wang, H.; Paulson, K.R.; Pease, S.A.; Watson, S.; Comfort, H.; Zheng, P.; Aravkin, A.Y.; Bisignano, C.; Barber, R.M.; Alam, T.; et al. Estimating excess mortality due to the COVID-19 pandemic: a systematic analysis of COVID-19-related mortality, 2020–21. *The Lancet* **2022**, *399*, 1513-1536, doi:https://doi.org/10.1016/S0140-6736(21)02796-3.
7. The pandemic's true death toll. Available online: https://www.economist.com/graphic-detail/coronavirus-excess-deaths-estimates (accessed on 26/09).
8. Lei, R.; Huo, R.; Mohan, C. Current and emerging trends in point-of-care urinalysis tests. *Expert Review of Molecular Diagnostics* **2020**, *20*, 69-84, doi:10.1080/14737159.2020.1699063.
9. Holmes, E.; Wilson, I.D.; Nicholson, J.K. Metabolic Phenotyping in Health and Disease. *Cell* **2008**, *134*, 714-717, doi:https://doi.org/10.1016/j.cell.2008.08.026.
10. Wu, D.; Shu, T.; Yang, X.; Song, J.-X.; Zhang, M.; Yao, C.; Liu, W.; Huang, M.; Yu, Y.; Yang, Q.; et al. Plasma metabolomic and lipidomic alterations associated with COVID-19. *National Science Review* **2020**, *7*, 1157-1168, doi:10.1093/nsr/nwaa086.
11. Barberis, E.; Amede, E.; Tavecchia, M.; Marengo, E.; Cittone, M.G.; Rizzi, E.; Pedrinelli, A.R.; Tonello, S.; Minisini, R.; Pirisi, M.; et al. Understanding protection from SARS-CoV-2 using metabolomics. *Scientific Reports* **2021**, *11*, 13796, doi:10.1038/s41598-021-93260-2.
12. Shen, B.; Yi, X.; Sun, Y.; Bi, X.; Du, J.; Zhang, C.; Quan, S.; Zhang, F.; Sun, R.; Qian, L.; et al. Proteomic and Metabolomic Characterization of COVID-19 Patient Sera. *Cell* **2020**, *182*, 59-72.e15, doi:https://doi.org/10.1016/j.cell.2020.05.032.
13. Villoslada, P.; Alonso, C.; Agirrezabal, I.; Kotelnikova, E.; Zubizarreta, I.; Pulido-Valdeolivas, I.; Saiz, A.; Comabella, M.; Montalban, X.; Villar, L.; et al. Metabolomic signatures associated with disease severity in multiple sclerosis. *Neurology - Neuroimmunology Neuroinflammation* **2017**, *4*, e321, doi:10.1212/nxi.0000000000000321.
14. Jacyna, J.; Kordalewska, M.; Artymowicz, M.; Markuszewski, M.; Matuszewski, M.; Markuszewski, M.J. Pre- and Post-Resection Urine Metabolic Profiles of Bladder Cancer Patients: Results of Preliminary Studies on Time Series Metabolomics Analysis. *Cancers* **2022**, *14*, 1210.
15. Huang, X.; Zeng, J.; Zhou, L.; Hu, C.; Yin, P.; Lin, X. A New Strategy for Analyzing Time-Series Data Using Dynamic Networks: Identifying Prospective Biomarkers of Hepatocellular Carcinoma. *Scientific Reports* **2016**, *6*, 32448, doi:10.1038/srep32448.

16. Li, Y.; Xue, H.; Fang, S.; Wang, G.; Wang, Y.; Wang, T.; Shi, R.; Wu, J.; Ma, Y. Time-series metabolomics insights into the progressive characteristics of 3,5-diethoxycarbonyl-1,4-dihydrocollidine-induced cholestatic liver fibrosis in mice. *Journal of Pharmaceutical and Biomedical Analysis* **2021**, *198*, 113986, doi:https://doi.org/10.1016/j.jpba.2021.113986.
17. Li, R.; He, H.; Fang, S.; Hua, Y.; Yang, X.; Yuan, Y.; Liang, S.; Liu, P.; Tian, Y.; Xu, F.; et al. Time Series Characteristics of Serum Branched-Chain Amino Acids for Early Diagnosis of Chronic Heart Failure. *Journal of Proteome Research* **2019**, *18*, 2121-2128, doi:10.1021/acs.jproteome.9b00002.
18. Beale, D.J.; Shah, R.; Karpe, A.V.; Hillyer, K.E.; McAuley, A.J.; Au, G.G.; Marsh, G.A.; Vasan, S.S. Metabolic Profiling from an Asymptomatic Ferret Model of SARS-CoV-2 Infection. *Metabolites* **2021**, *11*, 327, doi:https://doi.org/10.3390/metabo11050327.
19. Au, G.G.; Marsh, G.A.; McAuley, A.J.; Lowther, S.; Trinidad, L.; Edwards, S.; Todd, S.; Barr, J.; Bruce, M.P.; Poole, T.B.; et al. Characterisation and natural progression of SARS-CoV-2 infection in ferrets. *Scientific Reports* **2022**, *12*, 5680, doi:10.1038/s41598-022-08431-6.
20. Cevik, M.; Kuppalli, K.; Kindrachuk, J.; Peiris, M. Virology, transmission, and pathogenesis of SARS-CoV-2. **2020**, *371*, m3862, doi:10.1136/bmj.m3862 %J BMJ.
21. Muñoz-Fontela, C.; Widerspick, L.; Albrecht, R.A.; Beer, M.; Carroll, M.W.; de Wit, E.; Diamond, M.S.; Dowling, W.E.; Funnell, S.G.P.; García-Sastre, A.; et al. Advances and gaps in SARS-CoV-2 infection models. *PLOS Pathogens* **2022**, *18*, e1010161, doi:10.1371/journal.ppat.1010161.
22. Ryan, K.A.; Bewley, K.R.; Fotheringham, S.A.; Slack, G.S.; Brown, P.; Hall, Y.; Wand, N.I.; Marriott, A.C.; Cavell, B.E.; Tree, J.A.; et al. Dose-dependent response to infection with SARS-CoV-2 in the ferret model and evidence of protective immunity. *Nature Communications* **2021**, *12*, 81, doi:10.1038/s41467-020-20439-y.
23. Cogliati Dezza, F.; Oliva, A.; Cancelli, F.; Savelloni, G.; Valeri, S.; Mauro, V.; Calabretto, M.; Russo, G.; Venditti, M.; Turriziani, O.; et al. Determinants of prolonged viral RNA shedding in hospitalized patients with SARS-CoV-2 infection. *Diagnostic Microbiology and Infectious Disease* **2021**, *100*, 115347, doi:https://doi.org/10.1016/j.diagmicrobio.2021.115347.
24. Hu, X.; Xing, Y.; Jia, J.; Ni, W.; Liang, J.; Zhao, D.; Song, X.; Gao, R.; Jiang, F. Factors associated with negative conversion of viral RNA in patients hospitalized with COVID-19. *Science of the Total Environment* **2020**, *728*, 138812.
25. Cevik, M.; Tate, M.; Lloyd, O.; Maraolo, A.E.; Schafers, J.; Ho, A. SARS-CoV-2, SARS-CoV, and MERS-CoV viral load dynamics, duration of viral shedding, and infectiousness: a systematic review and meta-analysis. *The Lancet Microbe* **2021**, *2*, e13-e22, doi:https://doi.org/10.1016/S2666-5247(20)30172-5.
26. Agarwal, V.; Venkatakrishnan, A.J.; Puranik, A.; Lopez-Marquez, A.; Challener, D.W.; Horo, J.C.; Badley, A.D.; Halamka, J.D.; Morice, W.G.; Soundararajan, V. Quantifying the prevalence of SARS-CoV-2 long-term shedding among non-hospitalized COVID-19 patients. *MedRxiv* **2020**.
27. Gombar, S.; Chang, M.; Hogan, C.A.; Zehnder, J.; Boyd, S.; Pinsky, B.A.; Shah, N.H. Persistent detection of SARS-CoV-2 RNA in patients and healthcare workers with COVID-19. *Journal of Clinical Virology* **2020**, *129*, 104477.
28. Bojkova, D.; Costa, R.; Reus, P.; Bechtel, M.; Jaboreck, M.-C.; Olmer, R.; Martin, U.; Ciesek, S.; Michaelis, M.; Cinatl, J. Targeting the Pentose Phosphate Pathway for SARS-CoV-2 Therapy. **2021**, *11*, 699.
29. Mesri, E.A.; Lampidis, T.J. 2-Deoxy-d-glucose exploits increased glucose metabolism in cancer and viral-infected cells: Relevance to its use in India against SARS-CoV-2. **2021**, *73*, 1198-1204, doi:https://doi.org/10.1002/iub.2546.
30. Bai, X.; Narayanan, A.; Skagerberg, M.; Ceña-Diez, R.; Giske, C.G.; Strålin, K.; Sönnerborg, A. Characterization of the Upper Respiratory Bacterial Microbiome in Critically Ill COVID-19 Patients. **2022**, *10*, 982.
31. Forst, C.V.; Zeng, L.; Wang, Q.; Zhou, X.; Vatansever, S.; Tu, Z.; Zhang, B. Tissue Specific Age Dependence of the Cell Receptors Involved in the SARS-CoV-2 Infection. **2021**, 2021.2007.2013.452256, doi:10.1101/2021.07.13.452256 %J bioRxiv.
32. Wang, M.-Y.; Zhao, R.; Gao, L.-J.; Gao, X.-F.; Wang, D.-P.; Cao, J.-M. SARS-CoV-2: Structure, Biology, and Structure-Based Therapeutics Development. *Frontiers in Cellular and Infection Microbiology* **2020**, *10*, doi:10.3389/fcimb.2020.587269.

33. Sun, N.; Fernandez, I.E.; Wei, M.; Witting, M.; Aichler, M.; Feuchtinger, A.; Burgstaller, G.; Verleden, S.E.; Schmitt-Kopplin, P.; Eickelberg, O.; et al. Pharmacometabolic response to pirfenidone in pulmonary fibrosis detected by MALDI-FTICR-MSI. **2018**, *52*, 1702314, doi:10.1183/13993003.02314-2017 %J European Respiratory Journal.
34. Cao, W.; Feng, Q.; Wang, X. Computational analysis of TMPRSS2 expression in normal and SARS-CoV-2-infected human tissues. *Chemico-Biological Interactions* **2021**, *346*, 109583, doi:https://doi.org/10.1016/j.cbi.2021.109583.
35. Lodge, S.; Nitschke, P.; Kimhofer, T.; Wist, J.; Bong, S.-H.; Loo, R.L.; Masuda, R.; Begum, S.; Richards, T.; Lindon, J.C.; et al. Diffusion and Relaxation Edited Proton NMR Spectroscopy of Plasma Reveals a High-Fidelity Supramolecular Biomarker Signature of SARS-CoV-2 Infection. *Analytical Chemistry* **2021**, *93*, 3976-3986, doi:10.1021/acs.analchem.0c04952.
36. Krishnan, S.; Nordqvist, H.; Ambikan, A.T.; Gupta, S.; Sperk, M.; Svensson-Akusjärvi, S.; Mikaeloff, F.; Benfeitas, R.; Saccon, E.; Ponnan, S.M.; et al. Metabolic Perturbation Associated With COVID-19 Disease Severity and SARS-CoV-2 Replication. *Molecular & Cellular Proteomics* **2021**, *20*, doi:10.1016/j.mcpro.2021.100159.
37. Lawler, N.G.; Gray, N.; Kimhofer, T.; Boughton, B.; Gay, M.; Yang, R.; Morillon, A.-C.; Chin, S.-T.; Ryan, M.; Begum, S.; et al. Systemic Perturbations in Amine and Kynurenine Metabolism Associated with Acute SARS-CoV-2 Infection and Inflammatory Cytokine Responses. *Journal of Proteome Research* **2021**, *20*, 2796-2811, doi:10.1021/acs.jproteome.1c00052.
38. Li, W.; Hulswit, R.J.; Widjaja, I.; Raj, V.S.; McBride, R.; Peng, W.; Widagdo, W.; Tortorici, M.A.; Van Dieren, B.; Lang, Y. Identification of sialic acid-binding function for the Middle East respiratory syndrome coronavirus spike glycoprotein. *Proceedings of the National Academy of Sciences* **2017**, *114*, E8508-E8517.
39. Tortorici, M.A.; Walls, A.C.; Lang, Y.; Wang, C.; Li, Z.; Koerhuis, D.; Boons, G.-J.; Bosch, B.-J.; Rey, F.A.; de Groot, R.J. Structural basis for human coronavirus attachment to sialic acid receptors. *Nature structural & molecular biology* **2019**, *26*, 481-489.
40. Barberis, E.; Timo, S.; Amede, E.; Vanella, V.V.; Puricelli, C.; Cappellano, G.; Raineri, D.; Cittone, M.G.; Rizzi, E.; Pedrinelli, A.R. Large-Scale Plasma Analysis Revealed New Mechanisms and Molecules Associated with the Host Response to SARS-CoV-2. *International journal of molecular sciences* **2020**, *21*, 8623.
41. Bruzzone, C.; Bizkarguenaga, M.; Gil-Redondo, R.; Diercks, T.; Arana, E.; García de Vicuña, A.; Seco, M.; Bosch, A.; Palazón, A.; San Juan, I.; et al. SARS-CoV-2 Infection Dysregulates the Metabolomic and Lipidomic Profiles of Serum. *iScience* **2020**, *23*, 101645, doi:https://doi.org/10.1016/j.isci.2020.101645.
42. Li, G.; Wu, X.; Zhou, C.-l.; Wang, Y.-m.; Song, B.; Cheng, X.-b.; Dong, Q.-f.; Wang, L.-l.; You, S.-s.; Ba, Y.-m. Uric acid as a prognostic factor and critical marker of COVID-19. *Scientific Reports* **2021**, *11*, 17791, doi:10.1038/s41598-021-96983-4.
43. Pallister, J.; Middleton, D.; Crameri, G.; Yamada, M.; Klein, R.; Hancock, T.J.; Foord, A.; Shiell, B.; Michalski, W.; Broder, C.C. Chloroquine administration does not prevent Nipah virus infection and disease in ferrets. *Journal of virology* **2009**, *83*, 11979-11982.
44. Caly, L.; Druce, J.; Roberts, J.; Bond, K.; Tran, T.; Kostecki, R.; Yoga, Y.; Naughton, W.; Taiaroa, G.; Seemann, T. Isolation and rapid sharing of the 2019 novel coronavirus (SARS‐CoV‐2) from the first patient diagnosed with COVID‐19 in Australia. *Medical Journal of Australia* **2020**, *212*, 459-462.
45. Au, G.G.; Marsh, G.A.; McAuley, A.J.; Lowther, S.; Trinidad, L.; Edwards, S.; Todd, S.; Barr, J.; Bruce, M.P.; Poole, T.B.; et al. Characterisation and natural progression of SARS-CoV-2 infection in ferrets. *Scientific reports* **2022**, *12*, 5680-5680, doi:10.1038/s41598-022-08431-6.
46. Marsh, G.A.; McAuley, A.J.; Brown, S.; Pharo, E.A.; Crameri, S.; Au, G.G.; Baker, M.L.; Barr, J.A.; Bergfeld, J.; Bruce, M.P.; et al. In vitro characterisation of SARS-CoV-2 and susceptibility of domestic ferrets (Mustela putorius furo). *Transboundary and emerging diseases* **2022**, *69*, 297-307, doi:10.1111/tbed.13978.
47. Beale, D.J.; Shah, R.; Karpe, A.V.; Hillyer, K.E.; McAuley, A.J.; Au, G.G.; Marsh, G.A.; Vasan, S.S. Metabolic Profiling from an Asymptomatic Ferret Model of SARS-CoV-2 Infection. **2021**, *11*, 327.
48. Pang, Z.; Chong, J.; Zhou, G.; de Lima Morais, D.A.; Chang, L.; Barrette, M.; Gauthier, C.; Jacques, P.-É.; Li, S.; Xia, J. MetaboAnalyst 5.0: narrowing the gap between raw spectra and functional insights. *Nucleic acids research* **2021**, *49*, W388-W396.

49. Karpe, A.V.; Beale, D.J.; Morrison, P.D.; Harding, I.H.; Palombo, E.A. Untargeted metabolic profiling of *Vitis vinifera* during fungal degradation. *FEMS Microbiol. Lett.* **2015**, *362*, fnv060, doi:http://doi.org/10.1093/femsle/fnv060.
50. Barupal, D.K.; Fiehn, O. Chemical Similarity Enrichment Analysis (ChemRICH) as alternative to biochemical pathway mapping for metabolomic datasets. *Scientific Reports* **2017**, *7*, 14567, doi:10.1038/s41598-017-15231-w.

Preprints (www.preprints.org) | NOT PEER-REVIEWED | Posted: 21 October 2022 doi:10.20944/preprints202210.0320.v1

Appendix A

Table S1. Composition of QC mix standards (1 ppm) applied to assess the variability of the LC-QQQ-MS metabolomic analysis for central carbon metabolites.

QC Standard	RSD (%)
L-Arginine	6.11
L-Histidine	9.58
L-Proline	5.96
L-Serine	4.36
L-Cystine	7.39
L-Threonine	3.73
L-Homoserine	6.79
L-Methionine	4.76
L-Isoleucine	5.29
L-Leucine	4.51
L-Tyrosine	8.21
L-Glutamic acid	5.48
L-Phenylalanine	4.00
L-Aspartic Acid	3.33
Lactic acid	11.07
Succinic acid	4.40

Table S2. Composition of PBQC metabolites applied to assess the variability of the LC-QQQ-MS metabolomic analysis for central carbon metabolites.

PBQC metabolite	RSD (%)
L-Glutamine	8.23
4-Guanidobutyric acid	8.64
L-Tyrosine	7.85
Pyridoxal hydrochloride	8.75
Inosine	7.68
2-Deoxyinosine	5.78
L-Kynurenine	8.06
Guanosine	5.83
L-Glutamic acid	2.14
L-Phenylalanine	2.68
L-Aspartic Acid	2.30
Uric acid	9.28
Thymidine	7.15
D-Gluconic acid	4.32
Galactonic acid	4.21
L-Dihydroorotic acid	4.07
N-Acetyl-alpha-D-glucosamine 1-phosphate	8.82
N-Acetyl-D-glucosamine 6-phosphate	8.82
D-Sedoheptulose-7-phosphate	5.14
Nicotinic acid	9.29
4-Hydroxybenzoic acid	8.49
D-pantothenic acid	7.99
Maleic acid	9.66
Malonic acid	7.69

Preprints (www.preprints.org) | NOT PEER-REVIEWED | Posted: 21 October 2022 doi:10.20944/preprints202210.0320.v1

PBQC metabolite	RSD (%)
Succinic acid	1.77
Vanillic acid	9.72
m-Hydroxybenzoic acid	6.63
L-Malic acid	5.71
L-Hydroxyglutaric acid	6.12
N-Acetylglutamic acid	8.07
Isopentyl acetate	6.36
4-Hydroxyphenyl-pyruvic acid	8.81
D-Fructose 1,6-biphosphate	5.78
4-Pyridoxic acid	8.40

Note: Only metabolite features with RSDs ≤ 10% are represented in the table.

Table S3. Cross-validation (CV)-ANOVA of the PLS-DA metabolomics model (**Figure S2**)

PLS-DA (Figure S2)	SS	DF	MS	F-statistic	p-value	SD
Total corr.	400	400	1			1
Regression	24.3018	20	1.21509	1.229	0.226342	1.10231
Residual	375.698	380	0.98868			0.994324

In this table, SS: sum-of-squares, DF: degrees of freedom, MS: mean squares, SD: standard deviation

Table S4. Cross-validation (CV)-ANOVA of the OPLS-DA metabolomics model (**Figure 2**)

PLS-DA (Figure 2)	SS	DF	MS	F-statistic	p-value	SD
Total corr.	400	400	1			1
Regression	60.0163	40	1.50041	1.58874	0.0158789	1.22491
Residual	339.984	360	0.944399			0.971802

In this table, SS: sum-of-squares, DF: degrees of freedom, MS: mean squares, SD: standard deviation

 doi:10.20944/preprints202210.0320.v1

Table S5. Pathway enrichment analysis of the central carbon metabolic pathways using the central carbon metabolism dataset.

Metabolic pathway	Total	Expected	Hits	Raw p-value	Holm p-value	FDR	Enrichment ratio
Pentose phosphate pathway	22	1.17	7	<0.0001	0.00699	0.00699	5.982906
Pentose and glucuronate interconversions	18	0.958	6	0.0002	0.0174	0.00881	6.263048
Arginine biosynthesis	14	0.745	5	0.0005	0.0424	0.0145	6.711409
Starch and sucrose metabolism	18	0.958	5	0.0019	0.151	0.0373	5.219207
D-Glutamine and D-glutamate metabolism	6	0.319	3	0.0026	0.207	0.0373	9.404389
Alanine, aspartate and glutamate metabolism	28	1.49	6	0.0028	0.219	0.0373	4.026846
Citrate cycle (TCA cycle)	20	1.06	5	0.0031	0.243	0.0373	4.716981
Butanoate metabolism	15	0.798	4	0.0065	0.499	0.0625	5.012531
Valine, leucine and isoleucine biosynthesis	8	0.426	3	0.0067	0.509	0.0625	7.042254
Amino sugar and nucleotide sugar metabolism	37	1.97	6	0.0116	0.872	0.0977	3.045685
Phenylalanine, tyrosine and tryptophan biosynthesis	4	0.213	2	0.0157	1	0.12	9.389671
Glyoxylate and dicarboxylate metabolism	32	1.7	5	0.0244	1	0.171	2.941176
Nicotinate and nicotinamide metabolism	15	0.798	3	0.0416	1	0.269	3.759398
Ascorbate and aldarate metabolism	8	0.426	2	0.0636	1	0.381	4.694836
Phenylalanine metabolism	10	0.532	2	0.0954	1	0.534	3.759398
Galactose metabolism	27	1.44	3	0.1700	1	0.894	2.083333
Histidine metabolism	16	0.852	2	0.2080	1	1	2.347418
Aminoacyl-tRNA biosynthesis	48	2.55	4	0.2500	1	1	1.568627
Glycine, serine and threonine metabolism	33	1.76	3	0.2550	1	1	1.704545
Pantothenate and CoA biosynthesis	19	1.01	2	0.2680	1	1	1.980198
Nitrogen metabolism	6	0.319	1	0.2800	1	1	3.134796
Fructose and mannose metabolism	20	1.06	2	0.2890	1	1	1.886792
Propanoate metabolism	23	1.22	2	0.3490	1	1	1.639344
Taurine and hypotaurine metabolism	8	0.426	1	0.3550	1	1	2.347418
Purine metabolism	65	3.46	4	0.4590	1	1	1.156069
Inositol phosphate metabolism	30	1.6	2	0.4810	1	1	1.25
Glycerolipid metabolism	16	0.852	1	0.5850	1	1	1.173709
Pyrimidine metabolism	39	2.08	2	0.6250	1	1	0.961538
beta-Alanine metabolism	21	1.12	1	0.6850	1	1	0.892857
Sphingolipid metabolism	21	1.12	1	0.6850	1	1	0.892857
Glycolysis / Gluconeogenesis	26	1.38	1	0.7620	1	1	0.724638

 doi:10.20944/preprints202210.0320.v1

Metabolic pathway	Total	Expected	Hits	Raw p-value	Holm p-value	FDR	Enrichment ratio
Glutathione metabolism	28	1.49	1	0.7870	1	1	0.671141
Phosphatidylinositol signaling system	28	1.49	1	0.7870	1	1	0.671141
Porphyrin and chlorophyll metabolism	30	1.6	1	0.8090	1	1	0.625
Cysteine and methionine metabolism	33	1.76	1	0.8390	1	1	0.568182
Glycerophospholipid metabolism	36	1.92	1	0.8640	1	1	0.520833
Arginine and proline metabolism	38	2.02	1	0.8780	1	1	0.49505
Valine, leucine and isoleucine degradation	40	2.13	1	0.8910	1	1	0.469484
Tryptophan metabolism	41	2.18	1	0.8970	1	1	0.458716
Primary bile acid biosynthesis	46	2.45	1	0.9220	1	1	0.408163

 doi:10.20944/preprints202210.0320.v1

Table S6. Multivariate ANOVA analysis of a metabolomics-derived dataset of nasal wash samples collected from ferrets at several time-points.

Metabolite feature	KEGG ID	F-statistic	FDR	Fisher's LSD
D-Sedoheptulose-7-P	C05382	14.607	3.59E-08	14 dpi > Pre; 3 dpi > 5 dpi; 3 dpi > Pre; 7 dpi > 5 dpi; 5 dpi > Pre; 7 dpi > Pre; 9 dpi > Pre
N-Acetyl D-galactosamine	C01132	14.241	3.59E-08	14 dpi > 5 dpi; 14 dpi > Pre; 3 dpi > 5 dpi; 3 dpi > Pre; 5 dpi > Pre; 7 dpi > Pre; 9 dpi > Pre
Uric acid	C00366	10.425	3.55E-06	5 dpi > 14 dpi; Pre > 14 dpi; 5 dpi > 3 dpi; Pre > 3 dpi; 5 dpi > 7 dpi; 5 dpi > 9 dpi; 9 dpi > 7 dpi; Pre > 7 dpi; Pre > 9 dpi
Vanillic acid	C06672	7.475	0.000172	5 dpi > 14 dpi; Pre > 14 dpi; 5 dpi > 3 dpi; Pre > 3 dpi; 5 dpi > 7 dpi; 5 dpi > 9 dpi; Pre > 7 dpi
Taurine	C00245	7.438	0.000172	14 dpi > 3 dpi; 14 dpi > 7 dpi; 14 dpi > Pre; 3 dpi > Pre; 5 dpi > Pre; 7 dpi > Pre; 9 dpi > Pre
Phenylpyruvic acid	C00166	7.318	0.000172	5 dpi > 14 dpi; Pre > 14 dpi; 5 dpi > 3 dpi; Pre > 3 dpi; 5 dpi > 7 dpi; 5 dpi > 9 dpi; Pre > 7 dpi; Pre > 9 dpi
Nicotinic acid	C00253	6.868	0.000299	Pre > 14 dpi; Pre > 3 dpi; Pre > 5 dpi; Pre > 7 dpi; Pre > 9 dpi
L-2-Hydroxyglutaric acid	C02630	5.869	0.001277	5 dpi > 14 dpi; 7 dpi > 14 dpi; 9 dpi > 14 dpi; Pre > 14 dpi; 5 dpi > 3 dpi; Pre > 3 dpi; Pre > 7 dpi; Pre > 9 dpi
2,3-Dihydroxyisovalerate	C04039	5.806	0.001277	3 dpi > 14 dpi; 5 dpi > 14 dpi; 7 dpi > 14 dpi; 9 dpi > 14 dpi; Pre > 14 dpi; Pre > 3 dpi; Pre > 5 dpi; Pre > 7 dpi
Mevalonic acid	C00418	5.724	0.001315	3 dpi > 14 dpi; 5 dpi > 14 dpi; 7 dpi > 14 dpi; 9 dpi > 14 dpi; Pre > 14 dpi
D-pantothenic acid	C00864	5.506	0.001709	Pre > 14 dpi; Pre > 3 dpi; Pre > 5 dpi; Pre > 7 dpi; Pre > 9 dpi
Malonic acid	C00383	4.888	0.004381	3 dpi > 14 dpi; 3 dpi > 5 dpi; 3 dpi > 9 dpi; 3 dpi > Pre
2,3-Dihydroxybenzoic acid	C00196	4.766	0.004961	5 dpi > 14 dpi; 5 dpi > 3 dpi; Pre > 3 dpi; 5 dpi > 7 dpi; 5 dpi > 9 dpi; Pre > 7 dpi
L-Maltose	C00208	4.435	0.008063	Pre > 3 dpi; Pre > 5 dpi; Pre > 7 dpi; Pre > 9 dpi
L-Phenylalanine	C00079	4.149	0.012247	Pre > 14 dpi; Pre > 3 dpi; 5 dpi > 7 dpi; Pre > 7 dpi; Pre > 9 dpi
2-Deoxycytidine 5'-diP	C00705	4.018	0.014351	14 dpi > 3 dpi; 14 dpi > 5 dpi; 14 dpi > 7 dpi; 14 dpi > 9 dpi; 14 dpi > Pre; 7 dpi > Pre
3-Hydroxyanthranilic acid	C00632	3.948	0.015249	5 dpi > 3 dpi; 9 dpi > 3 dpi; 5 dpi > 7 dpi; 9 dpi > 7 dpi
Citramalic acid	C00815	3.744	0.019342	14 dpi > 3 dpi; 14 dpi > 5 dpi; 14 dpi > 7 dpi; 14 dpi > 9 dpi; 14 dpi > Pre
D-Galactosamine	C02262	3.697	0.019931	14 dpi > 3 dpi; 14 dpi > 5 dpi; 14 dpi > Pre; 7 dpi > Pre; 9 dpi > Pre
L-Malic acid	C00149	3.596	0.022602	3 dpi > 14 dpi; 3 dpi > 5 dpi; 3 dpi > 9 dpi; 3 dpi > Pre; 7 dpi > Pre
N-Acetylneuraminic acid	C19910	3.415	0.029465	3 dpi > Pre; 5 dpi > Pre; 9 dpi > Pre
Succinic acid	C00042	3.371	0.029911	Pre > 5 dpi; Pre > 7 dpi; Pre > 9 dpi
m-Hydroxybenzoic acid	C00587	3.356	0.029911	Pre > 3 dpi; Pre > 7 dpi; Pre > 9 dpi
L-Sorbose	C08356	3.332	0.029934	Pre > 3 dpi; Pre > 5 dpi; Pre > 7 dpi; Pre > 9 dpi

 doi:10.20944/preprints202210.0320.v1

Table S6 (*cont.*). Multivariate ANOVA analysis of a metabolomics-derived dataset of nasal wash samples collected from ferrets at several time-points.

Metabolite feature	KEGG ID	F-statistic	FDR	Fisher's LSD
L-Serine	C00716	3.259	0.032611	3 dpi > Pre; 5 dpi > Pre; 7 dpi > Pre
Glyceric acid	C00258	3.052	0.044086	3 dpi > 14 dpi; 5 dpi > 14 dpi; 7 dpi > 14 dpi; 9 dpi > 14 dpi; Pre > 14 dpi; Pre > 7 dpi
N-Acetyl-α-D-glucosamine 1-P	C04256	3.022	0.044086	5 dpi > 14 dpi; 9 dpi > 14 dpi; 5 dpi > Pre; 9 dpi > Pre
N-Acetyl-D-glucosamine 6-P	C00357	3.022	0.044086	5 dpi > 14 dpi; 9 dpi > 14 dpi; 5 dpi > Pre; 9 dpi > Pre

In this table, P: phosphate, Pre: Pre-infection, dpi: days post-infection

Table S7. Significant discovery metabolites observed through LC-QTOF-MS analysis

Metabolite	F-statistic	FDR	Formula	Observed Mass	Theoretical mass	Mass error (ppm)
2,3-Dimethylsuccinic acid	12.441	2.70E-07	C6 H10 O4	146.0577	146.058457	5.182856
(+)-Isomyristic acid	11.447	3.67E-07	C14 H28 O2	228.2089	228.209479	2.537149
Stearolic acid	11.383	3.67E-07	C18 H32 O2	280.2403	280.240779	1.709247
Monoolein	10.786	6.22E-07	C21 H40 O4	356.2925	356.293208	1.987131
3-hydroxy-hexadecanoic acid	9.7278	1.83E-06	C16 H32 O3	272.2353	272.235693	1.443604
2-Hexyldecanoic acid	6.0773	0.000285	C16 H32 O2	256.2402	256.240779	2.259594
Vanillylmandelic acid	4.5567	0.00322	C9 H10 O5	198.0548	198.053372	7.210126
Phthalic acid Mono-2-ethylhexyl Ester	3.6172	0.014693	C16 H22 O4	278.1514	278.152358	3.444156

In this table, FDR: false discovery rate.

 doi:10.20944/preprints202210.0320.v1

Table S8. Pathway enrichment and impact analysis of a metabolomics-derived dataset of nasal wash samples collected from ferrets. 12

Metabolic pathway	Total	Expected	Hits	Pathway enrichment analysis			Pathway impact analysis			
				Raw p-value	Holm p-value	FDR	Raw p-value	Holm p-value	FDR	Impact
Phenylalanine, tyrosine and tryptophan biosynthesis	4	0.0723	2	0.0019	0.1610	0.1610	0.0018	0.15516	0.1552	0.5000
Phenylalanine metabolism	10	0.1807	2	0.0134	1	0.5630	0.0130	1	0.5440	0.6190
Butanoate metabolism	15	0.2710	2	0.0296	1	0.6210	0.0286	1	0.8004	0.0000
Citrate cycle (TCA cycle)	20	0.3613	2	0.3120	1	1	0.0489	1	0.9776	0.0769
Pentose phosphate pathway	22	0.3974	2	0.0601	1	1	0.0582	1	0.9776	0.0278
Glyoxylate and dicarboxylate metabolism	32	0.5781	2	0.4510	1	1	0.1120	1	1	0.0794
Taurine and hypotaurine metabolism	8	0.1445	1	0.1380	1	1	0.1360	1	1	0.4286
Nicotinate and nicotinamide metabolism	15	0.2710	1	0.2440	1	1	0.2402	1	1	0.0000
Glycerolipid metabolism	16	0.2890	1	0.2580	1	1	0.2541	1	1	0.0935
Starch and sucrose metabolism	18	0.3252	1	0.2850	1	1	0.2811	1	1	0.0731
Terpenoid backbone biosynthesis	18	0.3252	1	ND	ND	ND	0.2811	1	1	0.1143
Pantothenate and CoA biosynthesis	19	0.3432	1	0.2990	1	1	0.2942	1	1	0.0071
Pyruvate metabolism	22	0.3974	1	ND	ND	ND	0.3322	1	1	0.0311
Propanoate metabolism	23	0.4155	1	0.3500	1	1	0.3445	1	1	0.0000
Alanine, aspartate and glutamate metabolism	28	0.5058	1	0.4080	1	1	0.4025	1	1	0.0000
Glycine, serine and threonine metabolism	33	0.5961	1	0.4620	1	1	0.4555	1	1	0.0242
Amino sugar and nucleotide sugar metabolism	37	0.6684	1	0.0285	1	0.6210	0.4947	1	1	0.0386
Pyrimidine metabolism	39	0.7045	1	0.5200	1	1	0.5132	1	1	0.0175
Tryptophan metabolism	41	0.7407	1	0.5380	1	1	0.5311	1	1	0.0516
Primary bile acid biosynthesis	46	0.8310	1	0.5800	1	1	0.5731	1	1	0.0076
Fatty acid biosynthesis	47	0.8490	1	ND	ND	ND	0.5810	1	1	0.0000
Aminoacyl-tRNA biosynthesis	48	0.8671	1	0.5960	1	1	0.5888	1	1	0.0000
Purine metabolism	65	1.1742	1	0.7090	1	1	0.7019	1	1	0.0000

In this table, ND: Not detected 13

Preprints (www.preprints.org) | NOT PEER-REVIEWED | Posted: 21 October 2022 doi:10.20944/preprints202210.0320.v1

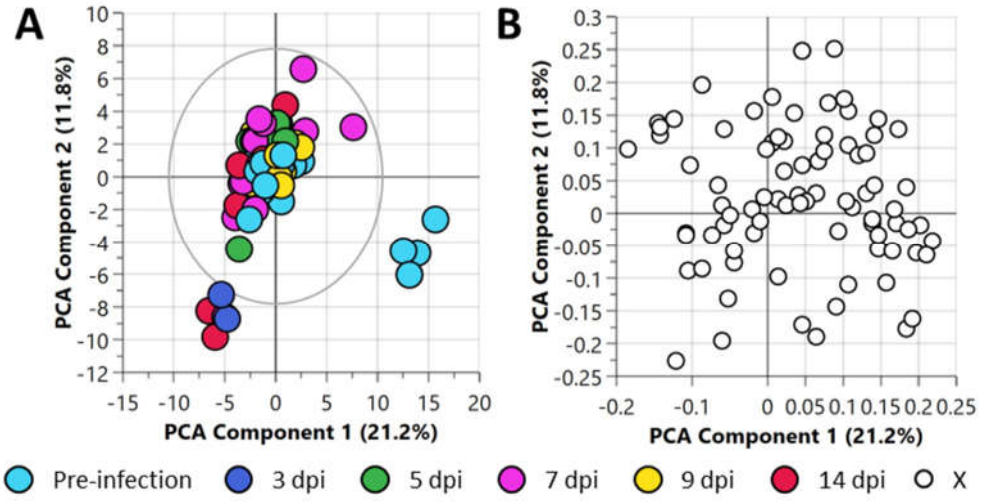

Figure S1. Principal component analysis (PCA) of the central carbon metabolism metabolite dataset of nasal wash samples collected from ferrets. **A.** PCA scatter plot, and **B.** PCA loadings plot. For this plot, R^2X (cum) = 0.525, Q^2 = 0.305. The ellipse presented in panel **A** represents Hotelling's T^2 confidence limit (95%). The colored circles in panel **A** represent each analyzed sample, while the white circles in panel **B** indicate the distribution of metabolite features between these groups.

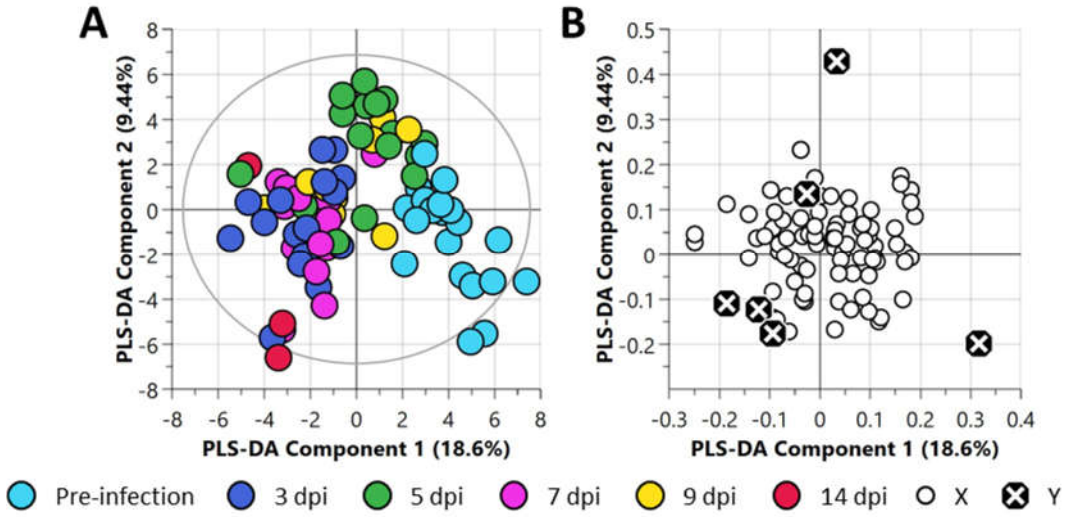

Figure S2. Partial least square discriminant analysis (PLS-DA) of the central carbon metabolism metabolite dataset of nasal wash samples collected from ferrets. **A.** PLS-DA scatter plot, and **B.** PLS-DA loadings plot. For this plot, R^2X (cum) = 0.28, R^2Y (cum) = 0.183, Q^2 = 0.0.06. The ellipse presented in panel **A** represents Hotelling's T^2 confidence limit (95%). The colored circles in panel **A** represent each analyzed sample, while the black crossed circles in panel **B** indicate the average group position for each sample cluster, with the white circles representing the distribution of metabolite features between these groups.